

Preparation, Properties, and Mechanism of Anionic and Cationic Cellulose Nanocrystals/Waterborne Polyurethane Composite Films

Ya-Yu Li,^a Yan-Ru Bai,^a Xin-Qian Zhang,^a Xin Liu,^a Zhen Dai,^a Ying-Long Jiang,^a Yi-Bo Yan,^a Zun-Qi Liu,^{a,*} Ming-Guo Ma^b

Three kinds of cellulose nanocrystals (CNCs) were added into waterborne polyurethane (WPU) and nanocomposite films that were prepared by solution casting. The influence of different ionic function groups on microstructure and properties of composite films was investigated. Compared with sulfated CNCs (SCNCs) and TEMPO oxidized CNCs (TOCNCs), FE-SEM images showed that cationized CNCs (CaCNCs) had better dispersion in composite films. The thermal decomposition of these composite films was delayed by 15 °C compared with pure WPU film. The tensile strength and fracture work of CaCNC/WPU composite film increased by 11.9% and 8.4%, respectively. The light transmittance of CaCNC/WPU composite film was highest among the 3 composite films, but its oxygen permeability was the lowest. In sum, the composite film with CaCNCs had optimal strength, toughness, light transmittance, and oxygen barrier properties, which is consistent with good compatibility of the two components and densest structure observed in SEM. There may be an ionic attraction and hydrogen bonds of CaCNCs and WPU in the composite film. The composite films are expected to have applications in food packaging, furniture coatings, and biomedical fields.

DOI: 10.15376/biores.18.1.447-464

Keywords: Cellulose nanocrystals; Waterborne polyurethane; Microstructure; Mechanical properties; Optical properties

Contact information: a: Xinjiang Key Laboratory of Agricultural Chemistry and Biomaterials, College of Chemistry and Chemical Engineering, Xinjiang Agricultural University, Urumqi 830052, Xinjiang Province, PR China; b: Engineering Research Center of Forestry Biomass Materials and Bioenergy, Beijing Key Laboratory of Lignocellulosic Chemistry, College of Materials Science and Technology, Beijing Forestry University, Beijing 100083, PR China; *Corresponding author: zunqi85@163.com

List of Abbreviations:

CNCs: cellulose nanocrystals
SCNCs: sulfated CNCs
TOCNCs: TEMPO oxidized CNCs
CaCNCs: cationized CNCs
WPU: waterborne polyurethane
PHBV: poly(3-hydroxybutyrate-co-3-hydroxyvalerate)
CNF: cellulose nanofiber
WVP: water vapor permeability
OP: oxygen permeability

The codes WC0, WSC10, WTC10, and WCC10 represent films pure WPU, WPU-SCNCs, WPU-TOCNCs, and WPU-CaCNCs films, respectively. SC, TC, and CC represent SCNCs, TOCNCs, and CaCNCs, respectively; 10 represents 10 wt% mass percentage of CNCs in the dry composite films.

INTRODUCTION

Cellulose nanocrystals (CNCs) are well-studied biomass nanoparticles due to their high annual availability, renewable properties, low cost, and excellent mechanical and optical properties (Foster *et al.* 2018). They have been investigated for tissue engineering (Sato *et al.* 2021), food packaging (Rader *et al.* 2021), optically active films (Zhang *et al.* 2021), and other applications (Li *et al.* 2018a).

In a previous study, CNCs with sulphate acid group were added into waterborne polyurethane (WPU) to prepare WPU/CNCs composites; the CNCs provided a significant enhancement to WPU films, including tensile strength and oxygen hindrance (Li *et al.* 2020b). At the same time, elongation at break and work of fracture of these nanocomposite films were reduced exponentially. The reason may be the weak interfacial force between filler and polymer matrix (Cao *et al.* 2007; Yu *et al.* 2017; Cheng *et al.* 2019).

Improving the interfacial compatibility between CNCs and WPU matrix and the interfacial bonding force is an urgent problem (Li *et al.* 2020a). Some studies added CNCs into monomer of WPU first and then reacted between them (Cao *et al.* 2009; Pei *et al.* 2011). Meesorn *et al.* (2017) added poly(vinyl alcohol) (PVOH) as compatibilizer between CNC and polymer matrix. Yu and Yao (2016) prepared three kinds of CNCs with different surface functional groups, and then added them to poly(3-hydroxybutyrate-co-3-hydroxyvalerate) (PHBV) separately. Because hydroxyl content on the surface of these three CNCs is different, the quantity of hydrogen bonds generated between CNCs and PHBV is different, too. With higher hydroxyl content, more hydrogen bonds form. The enhancement of intermolecular force will increase the tensile strength of the composite film. This biodegradable composite film can contribute to solving the problem of white pollution and will be applied to food packaging. Zhao *et al.* (2019) prepared CNCs with different ion content and added them into ionic polymers; the strength, dimensional stability, and proton conductivity of composite films were all improved. These films could be used in proton exchange field.

There have been many studies focusing on enhancement of polyelectrolyte composites by using nanoparticles carrying opposite signs of ionic charge. For example, Usuki *et al.* (1993) found that ion exchange and swelling method opens the layer space of bentonite. Tang *et al.* (2003) prepared organic-inorganic hybrid films considering ion crosslinking bond mechanism, *via* layer-by-layer assembly. They showed that the composite films have strength and toughness comparable to natural shells due to sacrificing ionic bonds, which greatly promoted the process from concept to practical application. Lodge (2008) proposed using ionic liquids for functional composite films preparation. The higher surface charge concentration at CNCs resulted in better mechanical reinforcement in CNCs/poly(acrylamide) nanocomposites (Yang *et al.* 2014). Wang *et al.* (2018b) added CNF with carboxyl to positively charged collagen fibers to fabricate composite films, which improved the tensile strength. The ion interaction mechanism is a potential method for preparation of composite films (Li *et al.* 2016; Fan *et al.* 2017). Araki (2013) pointed out that surface ionization of CNCs could keep its suspension stable. However, commercially available WPUs are generally anionic WPUs. Mixing ionized CNCs with WPUs is expected to produce composites with strong interfacial forces.

In this study, three kinds of ionized CNCs were used: sulfated CNCs (SCNCs) prepared by sulfuric acid method, TEMPO oxidized CNCs (TOCNCs), and cationic CNCs (CaCNCs). These three CNCs were mixed with WPU separately, and then CNC/WPU composite films were prepared by solution casting method. Various properties of the films

were systematically compared to explore the role of ion interaction mechanism in CNCs/WPU composite films.

EXPERIMENTAL

Materials

Three types of ionized CNCs are produced by sulfuric acid hydrolysis, TEMPO oxidation, and cationization. They were all purchased from Tianjin Woodelfbio Cellulose Co., Ltd. (Tianjin, China); their properties are shown in Table 1. Cotton dissolving pulp was used as raw material for CNC preparation. CaCNCs were prepared by reacting CNCs with (2,3-epoxypropyl)trimethylammonium chloride as shown by the literature (Eyley and Thielemans 2014). After the reaction of (2,3-epoxypropyl)trimethylammonium chloride with CNCs, a cationic group, ((2-hydroxyl, 3-oxyl)propyl) trimethylammonium chloride appeared on CNCs surface. Waterborne polyurethane (WPU, Model ADM-6161, 32.9% solid content) was kindly supplied by Shandong Audmay High Molecular Materials Co., Ltd. (Zibo, China).

Table 1. Three Kinds of Cellulose Nanocrystal (CNC) Suspension with Different Functional Groups

Category	Length (nm)	Diameter (nm)	Aspect Ratio	Surface Functional Group	Charge Density (mmol/g)
SCNCs	208	11	19	Sodium sulfate	0.642
TOCNCs	159	8	20	Carboxylic acid sodium	1.17
CaCNCs	196	10	20	((2-hydroxyl, 3-oxyl)propyl) trimethylammonium chloride	0.772

Category	Crystallinity Index	pH	Zeta Potential (mV)	Conductivity ($\mu\text{S}/\text{cm}$)	Suspension Concentration (wt.%)
SCNCs	90.3%	6.0-7.0	-54.2	600	1.47
TOCNCs	91.4%	7.0-8.0	-57.9	388	1.44
CaCNCs	88.7%	7.0-8.0	30.4	1048	0.78

Note: SCNCs: Sulfated CNCs; TOCNCs: TEMPO Oxidized CNCs; CaCNCs: Cationized CNCs;

As shown in Table 1, the surface charge contents of these three CNCs were different. The TOCNCs had the highest charge content, CaCNCs the next, and SCNCs the lowest. The pH of these CNC suspensions was approximately neutral. The crystallinity Index (*CrI*) of CaCNCs was slightly lower than the other two. This may be because CNCs are cationized in alkaline solution, resulting in a small fraction of crystal transformation occurring on surface (Eyley and Thielemans 2014).

Preparation of CNC/WPU Nanocomposite Films

Three kinds of CNCs were taken to prepare a mixture solution of CNCs and WPU. The dry weight ratio of CNCs to WPU was 10:90. The mixture was stirred by a magnetic rotor for 30 min and then poured into plastic Petri dishes of 120 cm length. The mixture was dried at room temperature for 30 days to obtain nanocomposite films. These films were pure WPU, WPU-SCNCs, WPU-TOCNCs, and WPU-CaCNCs films, and are coded as WC0, WSC10, WTC10, and WCC10, respectively. SC, TC, and CC represent SCNCs, TOCNCs, and CaCNCs, respectively; 10 represents 10 wt% mass percentage of CNCs in the dry composite films. The compositions are shown in Table 2.

Table 2. Composition of WPU (WC0) and Three CNC/WPU Films (WSC10, WTC10 and WCC10)

Films	Mass Fraction (%)			
	SCNCs	TOCNCs	CaCNCs	WPU
WC0	0	0	0	100
WSC10	10	0	0	90
WTC10	0	10	0	90
WCC10	0	0	10	90

Performance Testing

Thermogravimetry analysis

The instrument model was 209F3 (Netzsch, Selb, Germany). The weight of test samples was 10 ± 5 mg. The test temperature range was from room temperature to 600 °C. The heating rate was 10 °C/min, and the nitrogen flow rate was 50 mL/min.

Mechanical properties

A Universal mechanical testing machine (Zwick/Roell Z020, Zwick, Ulm, Germany) was mounted with 200 N load force assembly. Films were cut into rectangle specimens of 10 mm wide and 40 mm long. The thickness of the specimens was measured at the central position. The film was placed between two clamps that were 10.0 mm apart. The stretching rate was set at 5 mm/min. Five parallel samples were tested for each film composition. The mean and standard deviation values of elastic modulus, tensile strength, elongation at break, and work of fracture were calculated.

Light transmittance

Wavelength scanning was carried out by a spectrometer (UV2310 II, Shanghai Tianmei Scientific Instrument Co., Ltd., Shanghai, China). The transmittance was recorded between 200 and 1000 nm, and the transmittance-wavelength curves were drawn.

Surface hydrophilicity

The hydrophilicity of composite films was quantified by measuring the contact angle of deionized water on the films. A microsyringe was used to drop 5 μ L of deionized water onto the film. The contact angle photos were taken using a Dynamic Contact Angle Measuring Device (SL200KS, KINO Industries, (Boston, USA) equipped with a camera. The contact angle was calculated using the CAST2.0 software. Each film was measured 5 times, and the average value was adopted.

Hygroscopicity

The nanocomposite films were put into a vacuum drying oven containing anhydrous calcium chloride and dried for 24 h. The temperature was set at 50 °C, and the vacuum degree was set at 0.1 MPa. The dry weight of the nanocomposite films was recorded as w_1 (g). A 100 mL small beaker containing 20 mL water was placed in a 2 L beaker. The nanocomposite films were placed in the 2 L beaker, outside of the 100 mL small beaker. At last, the 2 L beaker was sealed with plastic wrap and put in a 30 °C thermostat (ZWYR-2102C, Shanghai Zhicheng Analytical Instrument Manufacturing Co., Ltd., Shanghai, China) to ensure a constant temperature and humidity (30.0 ± 0.3 °C, relative humidity RH of $99 \pm 1\%$). After 24 h, the weight of the film reaching hygroscopic balance was denoted as w_2 (g). Hygroscopicity was calculated as shown in Eq. 1.

$$\text{Hygroscopicity}[\%] = \frac{w_2 - w_1}{w_1} \times 100\% \quad (1)$$

Water vapor permeability

A simple experimental apparatus for measuring water vapor permeability was assembled as described previously (Li *et al.* 2020b). Nanocomposite film as mounted on the mouth of a small bottle containing anhydrous calcium chloride. The bottle was placed in a 2 L beaker, which was placed in a thermostat. The weight of the bottle was measured regularly. The water vapor permeability (WVP) was calculated as follows:

$$\text{Water absorption [g} \cdot \text{cm}/(\text{cm}^2 \cdot \text{Pa})] = \frac{W \cdot T}{A \cdot \Delta P} \quad (2)$$

where W is the mass of H₂O absorbed by calcium chloride in glass vial (g); T is the thickness of the film (cm); A is the effective area of the film (cm²); and ΔP is the pressure difference of water vapor between outside and inside of glass vial. The water saturated pressure at 30 °C was 4.2455 kPa, so the water vapor pressure outside of the glass vial was assumed to be 4.2455 kPa. The water vapor pressure inside of glass vial is 0 kPa, so $\Delta P = 4246$ Pa.

Oxygen permeability

A gas permeability meter (Basic 201, Jinan Labthink Instruments Co., Ltd., Jinan, China) was used to test oxygen transmission rate (OTR, cm³ (cm²·s·Pa)⁻¹). OTR multiplied by the thickness of nanocomposite film (cm) to get oxygen permeability of the thin film (OP, cm³·cm (cm²·s·Pa)⁻¹).

Structural Characterization Method*Fourier-transform infrared spectroscopy*

FTIR spectra were collected on an instrument (model Nicolet 6700, Thermo Fisher Company, Waltham, MA, USA) equipped with ATR component, in the range of 600 to 4000 cm⁻¹, using a scanning rate of 4 cm⁻¹ and 32 scans.

X-ray diffraction

The instrument model was X'Pert-Pro MPD (Panalytical, Malvern, UK). Cu target radiation was used (wavelength 0.154 nm, voltage 40 kV, current 40 mA). The composite film was tested in the 2θ range of 10° to 50°.

Field emission scanning electron microscope

A field emission scanning electron microscope (FE-SEM, model SU8010, Hitachi, Tokyo, Japan) was used to obtain surface and cross-sectional morphologies of the nanocomposite film. Voltage was set at 3 kV. A cross-sectional sample of film was prepared *via* quenching in liquid nitrogen. The samples were sprayed with gold before observation.

RESULTS AND DISCUSSION

Chemical Composition and Microstructure of Nanocomposite Films

FTIR study

Figure 1 shows FT-IR spectra of pure WPU film (WC0) and composite films with different ionized CNCs (WSC10, WTC10, and WCC10). The positions and intensities of most of absorption peaks of the four curves are the same. At 3332 cm^{-1} , the intensities are a little different in the four curves. This may be caused by different content of hydrogen bonds (Yu and Yao 2016). In Fig. 1(b), WSC10, WTC10, and WCC10 have new absorption peaks at 1161, 1110, 1059, and 1035 cm^{-1} , corresponding to the vibration peak of pyran ring of glucose in CNCs. These peaks do not appear in WC0 (Cao *et al.* 2007). This result indicates presence of CNCs in WSC10, WTC10, and WCC10.

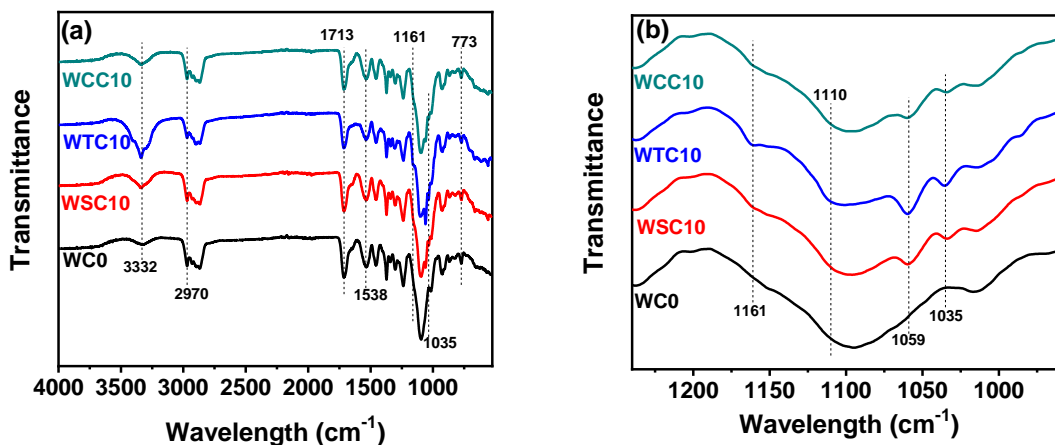


Fig. 1. FT-IR spectra of pure waterborne polyurethane (WPU) (WC0) and CNC/WPU films (WSC10, WTC10, and WCC10) with three kinds of CNCs

XRD study

Figure 2 shows XRD patterns of nanocomposite films. Pure WPU film had no crystalline peaks. After adding three CNCs, diffraction peaks appeared at $2\theta = 15.0^\circ$, 16.8° , and 22.9° . These crystalline peaks are all characteristic peaks of cellulose I. The diffraction peak of cellulose I at 34.5° does not appear due to low content of cellulose in these films (Cao *et al.* 2009). However, the new diffraction peaks appearing at 29.4° , 30.7° , 39.3° , and 47.4° are not characteristic peaks of cellulose. This phenomenon has not been reported previously (Marcovich *et al.* 2006; Cao *et al.* 2007; Wang *et al.* 2010; Pei *et al.* 2011; Hormaiztegui *et al.* 2016). Khan *et al.* (2012) prepared CNC/chitosan nanocomposite films. XRD showed that CNCs promoted crystallization of chitosan matrix due to the trans-crystal effect. Santamaria-Echart *et al.* (2016) showed that the crystallinity of WPU

increased, after 0.5% CNCs were added. Therefore, the new diffraction peaks at 29.4° , 30.7° , 39.3° , and 47.4° may be caused by CNCs induced WPU crystallization.

Fang *et al.* (2014) found two weak diffraction peaks at 18° and 42° 2θ in XRD pattern of PU. They proposed that these two peaks are characteristic of soft segments PPG in polyurethane. The diffraction peaks of PU at 27.8° and 29.2° 2θ were reported by Zhang *et al.* (2012). After addition of modified CNC, the intensities of these peaks increased; Zhang *et al.* (2012) did not supply the structure of PU. This black box about molecular structure of WPU makes the huge difficulty to confirm the new XRD peaks. Moreover, the intensity 29.4° 2θ was weak and at the same order of magnitude of the amorphous peak at 19.0° 2θ of WC0. In addition, the new XRD peaks are considerably sharper, and start at a higher 2θ value, than might be expected for a polymer. Another possibility is that the new XRD peaks at 29.4° , 30.7° , 39.3° , and 47.4° 2θ could be ascribed to a few impurities. In sum, more information is needed to confirm the new XRD peaks.

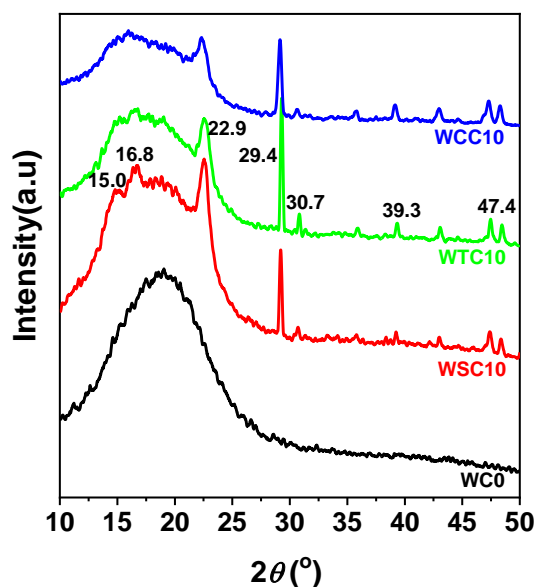


Fig. 2. XRD patterns of WPU (WC0) and CNC/WPU films (WSC10, WTC10, and WCC10) with three kinds of CNCs

SEM study

Figure 3 contains SEM images of the surfaces of nanocomposite films. The surface of film WC0 was very flat and dense. The surface of film WTC10 contains micron-dimension (Fig. 3. WTC10-1) and nano-dimension (Fig. 3. WTC10-3) cracks; these cracks indicate that compatibility between WPU and TOCNCs was very poor. The surface of film WSC10 was relatively flat and dense, but with some linear protrusions. These protrusions were dispersed CNCs, indicating that the compatibility between WPU and SCNCs was good. The surface of film WCC10 was smooth and dense, with some linear protrusions. These protrusions were also dispersed CNCs, indicating that compatibility between WPU and CaCNCs was also very good.

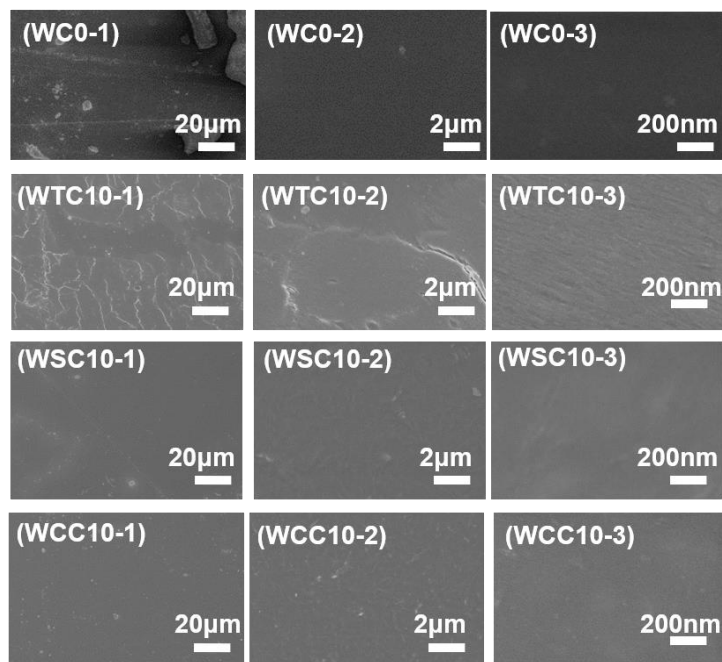


Fig. 3. FE-SEM micrographs of surface of WPU (WC0) and CNC/WPU films (WTC10, WSC10 and WCC10) with three kinds of CNCs

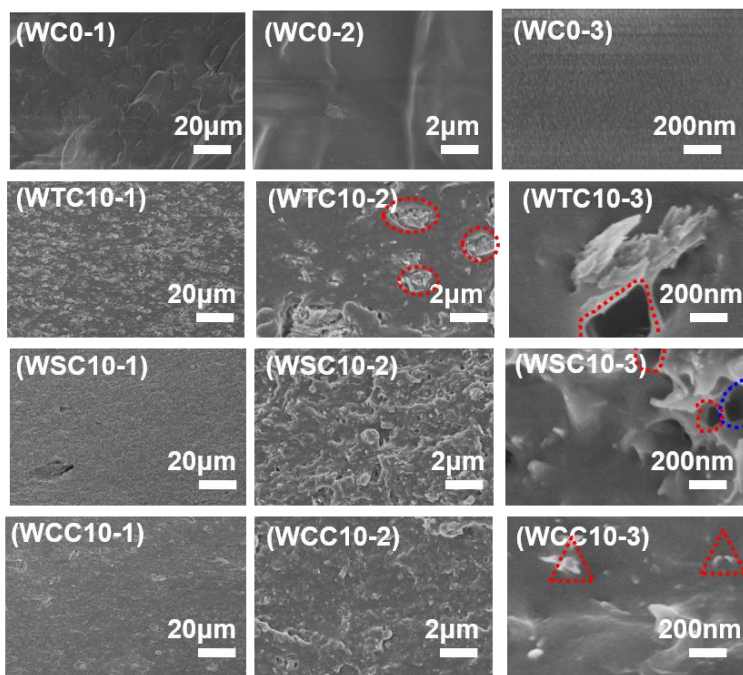


Fig. 4. FE-SEM micrographs of cross section of WPU (WC0) and CNC/WPU films (WTC10, WSC10 and WCC10) with three kinds of CNCs

Figure 4 shows cross-sectional SEM photographs of different nanocomposite films. The cross-section of pure WPU film WC0 only had micron-dimension flaky exfoliation. At nano-size, its cross section was very flat (Fig. 4, WC0-3). The cross-sections of three nanocomposite films were relatively rough in micron size (scale 20 μm , XXX-1). The cross

section of WTC10 was most rough, while WCC10 was a little rough. There were some TOCNCs agglomerates of about 1 μm size in WTC10 (photo WTC10-2), which can be explained as an island-like distribution of TOCNCs in the matrix. Photo WTC10-2 also confirms that roughness on photo WTC10-1 was caused by CNCs agglomerates. Pei *et al.* (2010) also observed SCNCs agglomerates of about 1 μm .

In photo WTC10-3 of Fig. 4, a cavity with diameter of about 200 nm was found (red dotted line). This cavity was produced due to the pulling out of an agglomerate. This result implies that the interface force between WPU and TOCNCs was poor. Some cavities were also observed in WSC10 but smaller, about 100 nm (red and blue dotted line, photo WSC10-3). However, no distinct cavity was found in WCC10 (photo WCC10-3).

According to the pullout mechanism of material fracture (Munch *et al.* 2008), these observation support that the interface binding force between WPU and CaCNCs was stronger. When CNCs have electric charge of same character as the WPU matrix, the CNCs tend to agglomerate into small patches due to electrostatic repulsion between CNCs and WPU. The formation of small patches will also be driven by the formation of hydrogen bonds between CNCs. Because TOCNCs carry about twice the negative charge of SCNCs, TOCNCs are easier to agglomerate than SCNCs. Pei *et al.* (2010) improved compatibility between CNCs and PLLA matrix through hydrophobic modification; finally, CNCs were dispersed uniformly in the matrix. Li *et al.* (2016) prepared CNCs with positive charges but different concentrations on its surface first. Then they added them to the matrix carboxymethyl cellulose. With gradually increasing surface charge of CNCs, the SEM results showed that CNCs dispersed more and more uniformly in the matrix. This result can be attributed to electrostatic repulsion between CNCs of the same charge. Like the principle of “*dissolution in the material of similar structure*”, charging of CNCs can also improve their dispersion in polymer matrix and result in stronger electrostatic interaction between molecules with different charges, at the same time. Finally, a composite film with better performance could be obtained.

Marcovich *et al.* (2006) and Cao *et al.* (2009) pointed out that the cross-section of nanocomposite film containing CNCs had dots. They assumed that these dots are cross-sections of CNCs. In XXX-3 of Fig. 4 (scale 200 nm), there are dot-like protrusions on the cross-sections of WSC10 and WCC10 (red dotted triangles). They should be also cross-sections of single CNCs exposed. This also supports that the dispersion of CNCs in films WSC10 and WCC10 was better than that in film WTC10.

Performance of Nanocomposite Films

Thermogravimetry study

Figure 5 shows thermogravimetric curves and thermogravimetric derivative curves of different nanocomposite films. When the temperature was below 200 $^{\circ}\text{C}$, WPU had almost no weight loss. This indicates that the commercially available WPU has good thermal stability. Pure WPU film had two main degradation peaks. The first degradation peak was at 337 $^{\circ}\text{C}$, representing degradation of hard chain segment in WPU; the second degradation peak was at 375 $^{\circ}\text{C}$, representing degradation of the soft chain in WPU (Liu *et al.* 2018). When 10 wt% various CNCs were added, the second degradation peak was increased from 375 $^{\circ}\text{C}$ to 390 $^{\circ}\text{C}$, indicating that degradation of WPU was delayed for 15 $^{\circ}\text{C}$ by three types of CNCs. CNC has a strong affinity to soft segment diol and induces its crystallization (Antolin-Ceron *et al.* 2022; Gupta and Mekonnen 2022). Yu and Yao (2016) added three kinds of CNCs with different surface hydroxyl content to PHBV matrix. The addition of CNCs increased T_{max} of PHBV by 48 $^{\circ}\text{C}$. They explained that as more hydrogen

bonds formed between the CNCs and matrix, the thermal stability of composite film is improved. As indicated in our early literature (Li *et al.* 2018b), CNCs would decomposed greatly into a char layer at around 350 °C. This char layer would cover on the adjacent WPU and delay its decomposition peak to 390 °C.

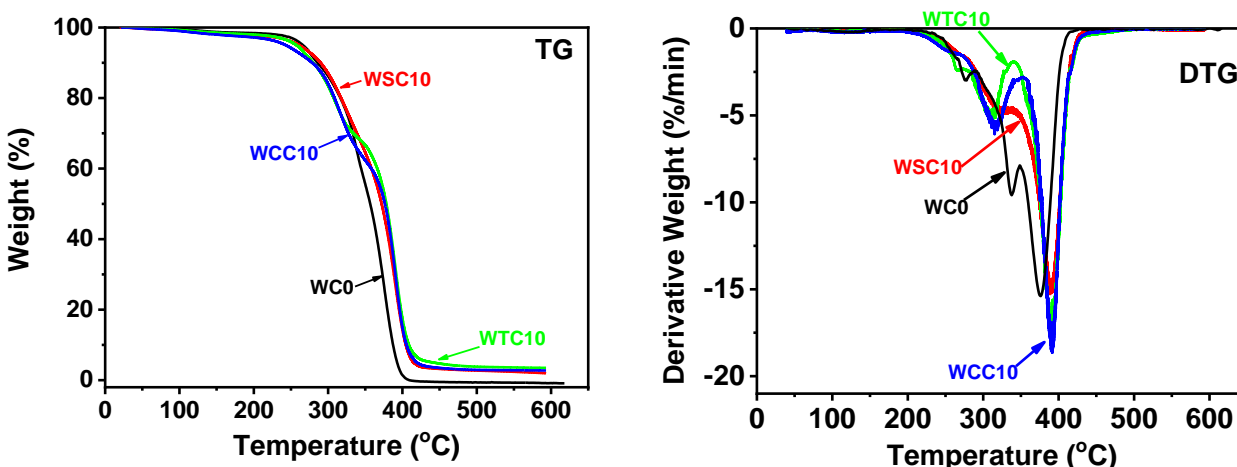


Fig. 5. Thermal-gravimetric (TG) and derivative thermal-gravimetric (DTG) curves of WPU (WC0) and CNC/WPU films (WSC10, WTC10 and WCC10) with three kinds of CNCs

Mechanical performance

Figure 6(a) shows the stress-strain curves of different nanocomposite films. The information of elastic modulus, tensile strength, elongation at break, and work of fracture were extracted from these stress-strain curves, and the average values and standard deviation were calculated to make histograms, as shown in Fig. 6(b-e). Figure 6(b) shows that after adding each of the three CNCs, the elastic modulus of all 3 composite films were improved, and the composite film added with SCNCs increased most of all that is 71.3%. Figure 6(c) shows that tensile strength of the composite film added with SCNCs and TOCNCs decreased, and tensile strength of the composite film added with CaCNCs improved, with an increase of 11.9%. Figure 6(d) shows that elongation at break of composite films added with three CNCs decreased, and that of the composite film added with SCNCs decreased most of all, by 42.8%; the elongation at break of composite film added with TOCNCs decreased moderately, by 34.5%; the elongation at break of composite film added with CaCNCs decreased least of all, by 11.1%. Figure 6(e) shows that work of fracture of composite films added with SCNCs and TOCNCs decreased. Work of fracture of the composite film added with TOCNCs decreased most of all, by 26.7%, while that of the composite film added with CaCNCs increased by 8.4%. Li *et al.* (2019) added chitosan and copper ions into CNFs; tensile strength and elastic modulus of the prepared composite films were increased by 104% and 75%, respectively. What is even more impressive is that compared with pure CNFs film, toughness of the composite film increased by 560%. The authors believe that this is the result of dual effects of hydrogen bonding and ion coordination among the three components in composites.

Overall, the composite film with CaCNCs exhibited the highest strength and toughness. The CaCNCs in WCC10 composite film were evenly dispersed in the matrix and had the best interfacial compatibility with matrix. This is consistent with the SEM characterization results.

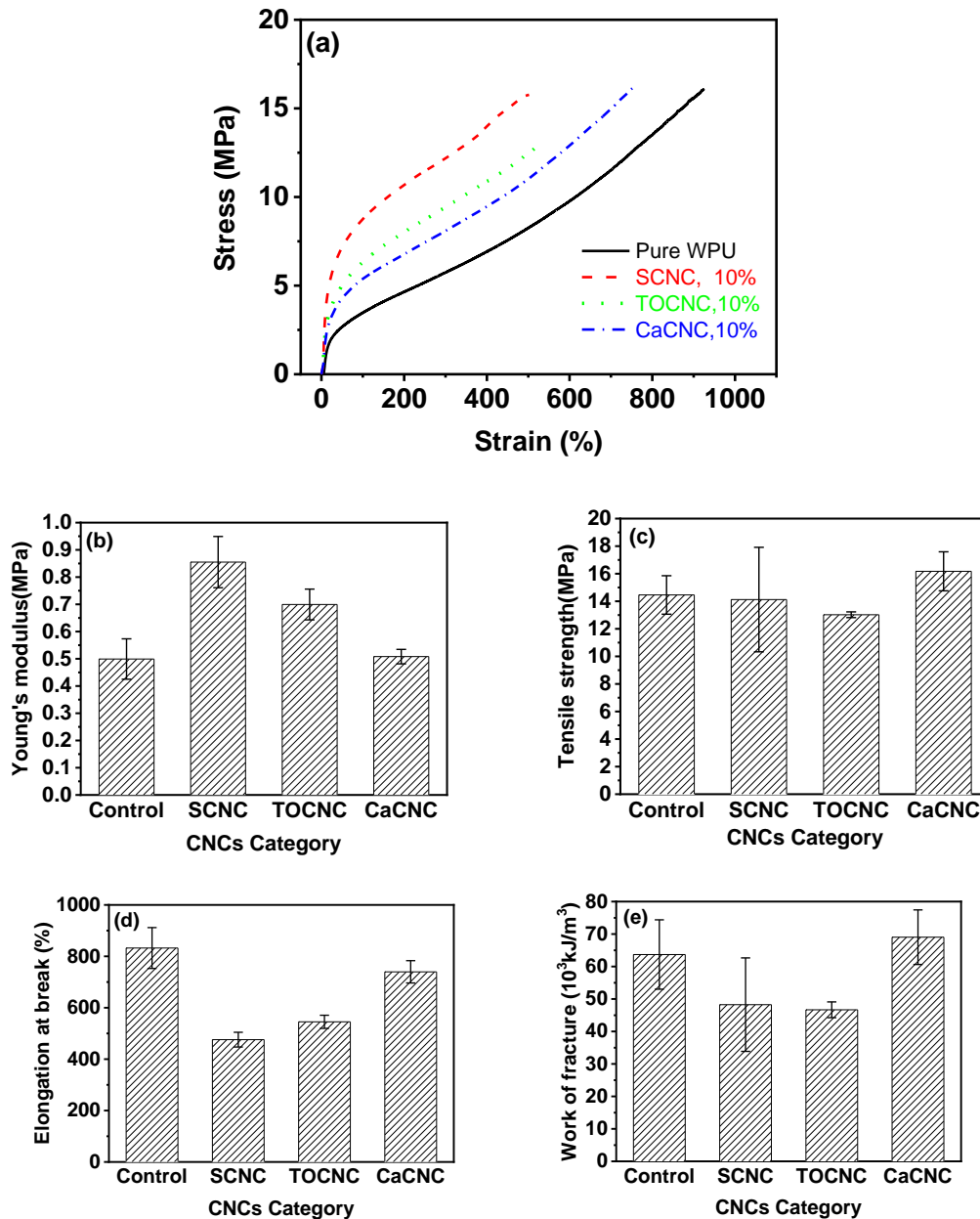


Fig. 6. Typical stress-strain curves (a), Young's modulus (b), tensile strength (c), elongation at break (d), and work of fracture (e) of WPU (control) and CNC/WPU films with three kinds of CNCs (The CNC category was marked in figure. The CNC content is 10 wt.% in all 3 composite films)

Appearance and UV-vis spectra study

Figure 7 is a photograph of different nanocomposite films. These composite films exhibited a smooth surface and good light transmittance. Pure WPU film had the highest light transmittance, but there were some wrinkles on its surface. Composite film with TOCNCs had the lowest light transmittance. Figure 8 shows the UV-vis spectra of different nanocomposite films. After CNCs were added, the light transmittance of composite films decreased; the light transmittance of composite film with TOCNCs decreased the most. This is because TOCNCs were unevenly distributed in the film, and the film surface had many micron-sized and nano-sized cracks. This phenomenon is also apparent in SEM photographs in Fig. 3. The light transmittance of composite film with CaCNCs was highest among the three composite films, which is consistent with good compatibility of the two components and densest structure observed in SEM of Fig. 4 (Yano *et al.* 2005; Girouard *et al.* 2016).

The result shown in Fig. 8 is also consistent with Fig. 7. Girouard *et al.* (2016) blended modified and unmodified CNCs with PU to prepare films. The modification changed the appearance of film from white to transparent. The authors explored reasons for the change in appearance of films and believed that this was due to the uniformly dispersed CNCs in PU matrix after modification.



Fig. 7. The appearance pictures of WPU (WC0) and CNC/WPU films (WTC10, WSC10 and WCC10) with three kinds of CNCs

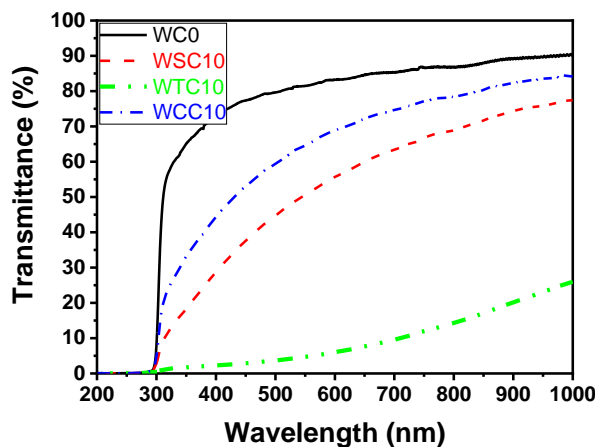


Fig. 8. The UV-vis spectra of WPU (WC0) and CNC/WPU films (WSC10, WTC10 and WCC10) with three kinds of CNCs

Surface hydrophilicity study

Table 3 shows contact angles of different nanocomposite films. By taking pure WPU film as a control, the contact angle of nanocomposite films decreased due to addition of CNCs. CNCs contain many hydroxyl groups, which have strong hydrophilicity and enhance hydrophilicity of films. Among them, hydrophilicity of WTC10 film increased the most. This is because there are many cracks on the surface of WTC10 film. Water droplets are easily immersed in a rough surface (Liu *et al.* 2017). Hydrophilicity of WCC10 film is lower than WTC10 film. The hydrophilicity of the WSC10 film was the lowest. This may be due to the higher charge content and lower crystallinity of CaCNCs, compared to SCNCs (Aulin *et al.* 2009).

Table 3. Contact Angle of WPU (WC0) and CNC/WPU Films (WSC10, WTC10 and WCC10) with Three Kinds of CNCs

Films	WC0	WSC10	WTC10	WCC10
Contact angle (°)	83.0	74.3	28.1	64.4

Hygroscopicity and water vapor permeability study

Figure 9 shows the hygroscopicity of different nanocomposite films. Hygroscopicity of film with cationic CNCs was the largest. This may be because the CaCNCs have lowest crystallinity and are most easily swelled by water vapor among the three types of CNCs (Aulin *et al.* 2009).

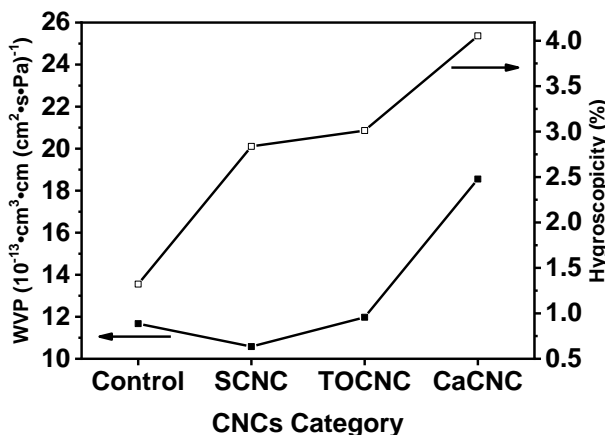


Fig. 9. Hygroscopicity and WVP of WPU and CNC/WPU films with three kinds of CNCs (The CNC category was marked in figure. The CNC content is 10 wt% in all 3 composite films)

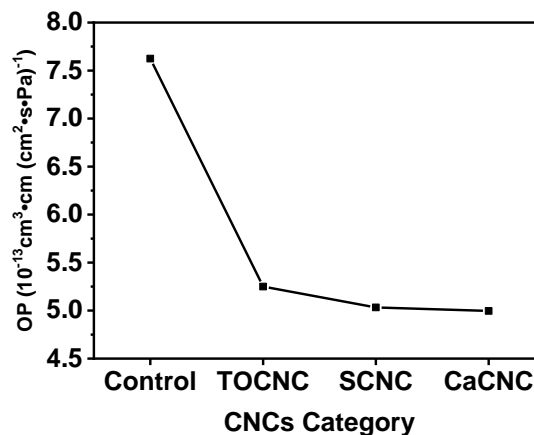


Fig. 10. The OP of WPU and CNC/WPU films with three kinds of CNCs (The CNC category was marked in figure. CNC content is 10 wt% in all 3 composite films)

Figure 9 also shows water vapor permeability (WVP) of different nanocomposite films. The WVP of composite film with SCNCs decreased. The WVP of composite film with TOCNCs increased slightly, and WVP of composite film with CaCNCs increased significantly. This is consistent with slight increase of hygroscopicity of WPU/TOCNC composite film and a large increase of hygroscopicity of WPU/CaCNC composite film. Therefore, WVP of composite film may have a close positive correlation with its hygroscopicity. Kumar *et al.* (2014) reached the same conclusion. Wang *et al.* (2018a) also

analyzed some parameters for the mechanism of WVP change of composite films containing nanocellulose. They carried out detailed investigations on three films of cellulose pure film, cellulose coated film, and cellulose reinforced film. The barrier properties of cellulose to water vapor are relatively poor. To achieve good water vapor barrier properties, materials with low WVP coefficient such as polyethylene should be used with nanocellulose to form a sandwich structure. Compared with the currently widely used synthetic plastics, this multilayer composite material has great competitive potential in the packaging materials market.

Oxygen permeability study

Figure 10 shows the oxygen permeability (OP) of different nanocomposite films. After adding three kinds of ionized CNCs, the OP of films decreases greatly. This is because CNCs are highly crystalline nanoparticles, and their addition can make oxygen transmission path tortuous. Among these 3 nanocomposite films, the oxygen permeability of film with cationic CNCs was the lowest, $5.00 \text{ cm}^3 \cdot \text{cm} (\text{cm}^2 \cdot \text{s} \cdot \text{Pa})^{-1}$, which was 34.4% lower than the control film. This may be due to that the structure of composite film with cationic CNCs is denser than the others. So, the presence of CaCNCs makes the path of oxygen passing through film more tortuous than that of other CNCs (Wang *et al.* 2018a). Compared with composite films WSC10 and WCC10, OP of WTC10 film is slightly higher. This may be caused by the uneven distribution of TOCNCs in the film. Because of uneven distribution of TOCNCs in the film, the local area with a low concentration of nanoparticles will become a channel for oxygen permeation (Wang *et al.* 2018b).

CONCLUSIONS

1. Three cellulose nanocrystal/water-borne polyurethane (CNC/WPU) composite films consisting of water-based polyurethane (WPU) and three different ionized cellulose nanocrystals (CNCs) were prepared by casting method. Compared with pure WPU control sample, thermal decomposition of composite films was delayed by 15 °C. FE-SEM results showed that cationized CNCs (CaCNCs) were uniformly distributed in matrix, and the composite film structure was dense.
2. Tensile strength of composite film with CaCNCs increased by 11.9%, and work of fracture increased by 8.4%, which were all optimal values of the three composite films. Composite film with CaCNCs had the highest optical transmittance, too. The OP value of film with CaCNCs decreased most, by 34.4%.
3. Comprehensive performance of CaCNC/WPU composite film was best of all. The mechanism may be: CaCNCs are nanoparticles with positive surface charge, while WPU is a polymer emulsion with bound anionic groups; there are opposite ion attraction and superimposed hydrogen bonding between them. These components interactions ultimately make structure of composite film compact. The prepared composite material is expected to find applications in food packaging, furniture coatings and biomedicine.

ACKNOWLEDGMENTS

This project was financially supported by the Key R&D Program of Xinjiang Uygur Autonomous Region (No. XJ20220264-3), Xinjiang Key Laboratory of Agricultural Chemistry and Biomaterials of Xinjiang Agricultural University (No. XJKF202205), and the research program of National Natural Science Foundation of China (No. 51863021).

REFERENCES CITED

- Antolin-Ceron, V.-H., Gonzalez-Lopez, F.-J., Astudillo-Sanchez, P. D., Barrera-Rivera, K.-A., and Martinez-Richa, A. (2022). "High-performance polyurethane nanocomposite membranes containing cellulose nanocrystals for protein separation," *Polymers* 14(4), 831. DOI: 10.3390/polym14040831
- Araki, J. (2013). "Electrostatic or steric? - preparations and characterizations of well-dispersed systems containing rod-like nanowhiskers of crystalline polysaccharides," *Soft Matter* 9(16), 4125-4141. DOI: 10.1039/c3sm27514k
- Aulin, C., Ahola, S., Josefsson, P., Nishino, T., Hirose, Y., Osterberg, M., and Wagberg, L. (2009). "Nanoscale cellulose films with different crystallinities and mesostructures – their surface properties and interaction with water," *Langmuir* 25(13), 7675-7685. DOI: 10.1021/la900323n
- Cao, X. D., Dong, H., and Li, C. M. (2007). "New nanocomposite materials reinforced with flax cellulose nanocrystals in waterborne polyurethane," *Biomacromolecules* 8(3), 899-904. DOI: 10.1021/bm0610368
- Cao, X. D., Habibi, Y., and Lucia, L. A. (2009). "One-pot polymerization, surface grafting, and processing of waterborne polyurethane-cellulose nanocrystal nanocomposites," *J. Mater. Chem.* 19(38), 7137-7145. DOI: 10.1039/b910517d
- Cheng, G., Zhou, M., Wei, Y.-J., Cheng, F., and Zhu, P.-X. (2019). "Comparison of mechanical reinforcement effects of cellulose nanocrystal, cellulose nanofiber, and microfibrillated cellulose in starch composites," *Polym. Composite.* 40(S1), E365-E372. DOI: 10.1002/pc.24685
- Eyley, S., and Thielemans, W. (2014). "Surface modification of cellulose nanocrystals," *Nanoscale* 6(14), 7764-7779. DOI: 10.1039/c4nr01756k
- Fan, J., Li, T., Ren, Y. Z., Qian, X. R., Wang, Q. W., Shen, J., and Ni, Y. H. (2017). "Interaction between two oppositely charged starches in an aqueous medium containing suspended mineral particles as a basis for the generation of cellulose-compatible composites," *Ind. Crop. Prod.* 97, 417-424. DOI: 10.1016/j.indcrop.2016.12.048
- Fang, C., Zhou, X., Yu, Q., Liu, S., Guo, D., Yu, R., and Hu, J. (2014). "Synthesis and characterization of low crystalline waterborne polyurethane for potential application in water-based ink binder," *Prog. Org. Coat.* 77(1), 61-71. DOI: 10.1016/j.porgcoat.2013.08.004
- Foster, E. J., Moon, R. J., Agarwal, U. P., Bortner, M. J., Bras, J., Camarero-Espinosa, S., Chan, K. J., Clift, M. J. D., Cranston, E. D., Eichhorn, S. J., Fox, D. M., Hamad, W. Y., Heux, L., Jean, B., Korey, M., Nieh, W., Ong, K. J., Reid, M. S., Renneckar, S., Roberts, R., Shatkin, J. A., Simonsen, J., Stinson-Bagby, K., Wanasekara, N., and Youngblood, J. (2018). "Current characterization methods for cellulose nanomaterials," *Chem. Soc. Rev.* 47(8), 2609-2679. DOI: 10.1039/c6cs00895j

- Girouard, N. M., Xu, S. H., Schueneman, G. T., Shofner, M. L., and Meredith, J. C. (2016). "Site-selective modification of cellulose nanocrystals with isophorone diisocyanate and formation of polyurethane-CNC composites," *ACS Appl. Mater. Inter.* 8(2), 1458-1467. DOI: 10.1021/acsami.5b10723
- Gupta, A., and Mekonnen, T. H. (2022). "Cellulose nanocrystals enabled sustainable polycaprolactone based shape memory polyurethane bionanocomposites," *J. Colloid. Interf. Sci.* 611, 726-738. DOI: 10.1016/j.jcis.2021.11.174
- Hormaiztegui, M. E. V., Lujan Mucci, V., Santamaria-Echart, A., Angeles Corcuera, M., Eceiza, A., and Ines Aranguren, M. (2016). "Waterborne polyurethane nanocomposites based on vegetable oil and microfibrillated cellulose," *J. Appl. Polym. Sci.* 133(47), article number 44207. DOI: 10.1002/app.44207
- Khan, A., Khan, R. A., Salmieri, S., Le Tien, C., Riedl, B., Bouchard, J., Chauve, G., Tan, V., Kamal, M. R., and Lacroix, M. (2012). "Mechanical and barrier properties of nanocrystalline cellulose reinforced chitosan based nanocomposite films," *Carbohydr. Polym.* 90(4), 1601-1608. DOI: 10.1016/j.carbpol.2012.07.037
- Kumar, V., Bollstrom, R., Yang, A., Chen, Q. X., Chen, G., Salminen, P., Bousfield, D., and Toivakka, M. (2014). "Comparison of nano- and microfibrillated cellulose films," *Cellulose* 21(5), 3443-3456. DOI: 10.1007/s10570-014-0357-5
- Li, M. C., Mei, C. T., Xu, X. W., Lee, S., and Wu, Q. L. (2016). "Cationic surface modification of cellulose nanocrystals: Toward tailoring dispersion and interface in carboxymethyl cellulose films," *Polymer* 107, 200-210. DOI: 10.1016/j.polymer.2016.11.022
- Li, S. F., Wen, X. N., Ju, W. L., Su, Y. L., and Wang, D. J. (2020a). "Effects of particle-polymer interactions and particle-particle interactions on mechanical properties of polymer nanocomposites," *Acta Polymerica Sinica* 52, 146-157. DOI: 10.11777/j.issn1000-3304.2020.20189
- Li, T., Zhang, X., Lacey, S. D., Mi, R., Zhao, X., Jiang, F., Song, J., Liu, Z., Chen, G., Dai, J., Yao, Y., Das, S., Yang, R., Briber, R. M., and Hu, L. (2019). "Cellulose ionic conductors with high differential thermal voltage for low-grade heat harvesting," *Nat. Mater.* 18, 608-613. DOI: 10.1038/s41563-019-0315-6
- Li, Y.-Y., Jing, W.-W., Wang, J.-H., and Li, J.-F. (2020b). "Elucidating the relationship between structure and property of WPU-CNCs nanocomposite films," *Sci. Adv. Mater.* 12(8), 1213-1224. DOI: 10.1166/sam.2020.3767
- Li, Y. Y., Wang, B., Ma, M. G., and Wang, B. (2018a). "Review of recent development on preparation, properties, and applications of cellulose-based functional materials," *Int. J. Polym. Sci.* 10(2), 1-19. DOI: 10.1155/2018/8973643
- Li, Y. Y., Wang, B., Ma, M. G., and Wang, B. (2018b). "The influence of pre-treatment time and sulfuric acid on cellulose nanocrystals," *BioResources* 13(2), 3585-3602. DOI: 10.15376/biores.13.2.3585-3602
- Liu, M., Wang, S., and Jiang, L. (2017). "Nature-inspired superwettability systems," *Nat. Rev. Mater.* 2, 1-17. DOI: 10.1038/natrevmats.2017.36
- Liu, Z. M., Wu, B., Jiang, Y. Y., Lei, J. X., Zhou, C. L., Zhang, J. H., and Wang, J. L. (2018). "Solvent-free and self-catalysis synthesis and properties of waterborne polyurethane," *Polymer* 143, 129-136. DOI: 10.1016/j.polymer.2018.04.010
- Lodge, T. P. (2008). "Materials science - A unique platform for materials design," *Science* 321(5885), 50-51. DOI: 10.1126/science.1159652
- Marcovich, N. E., Auad, M. L., Bellesi, N. E., Nutt, S. R., and Aranguren, M. I. (2006). "Cellulose micro/nanocrystals reinforced polyurethane," *J. Mater. Res.* 21(4), 870-

881. DOI: 10.1557/jmr.2006.0105
- Meesorn, W., Shirole, A., Vanhecke, D., de Espinosa, L. M., and Weder, C. (2017). "A simple and versatile strategy to improve the mechanical properties of polymer nanocomposites with cellulose nanocrystals," *Macromolecules* 50(6), 2364-2374. DOI: 10.1021/acs.macromol.6b02629
- Munch, E., Launey, M. E., Alsem, D. H., Saiz, E., Tomsia, A. P., and Ritchie, R. O. (2008). "Tough, bio-inspired hybrid materials," *Science* 322(5907), 1516-1520. DOI: 10.1126/science.1164865
- Pei, A. H., Malho, J. M., Ruokolainen, J., Zhou, Q., and Berglund, L. A. (2011). "Strong nanocomposite reinforcement effects in polyurethane elastomer with low volume fraction of cellulose nanocrystals," *Macromolecules* 44(11), 4422-4427. DOI: 10.1021/ma200318k
- Pei, A. H., Zhou, Q., and Berglund, L. A. (2010). "Functionalized cellulose nanocrystals as biobased nucleation agents in poly(L-lactide) (PLLA) - crystallization and mechanical property effects," *Compos. Sci. Technol.* 70(5), 815-821. DOI: 10.1016/j.compscitech.2010.01.018
- Rader, C., Weder, C., and Marti, R. (2021). "Biobased polyester-amide/cellulose nanocrystal nanocomposites for food packaging," *Macromol. Mater. Eng.* 306(3), article no. 2000668. DOI: 10.1002/mame.202000668
- Santamaria-Echart, A., Ugarte, L., Garcia-Astrain, C., Arbelaz, A., Angeles Corcuera, M., and Eceiza, A. (2016). "Cellulose nanocrystals reinforced environmentally-friendly waterborne polyurethane nanocomposites," *Carbohydr. Polym.* 151, 1203-1209. DOI: 10.1016/j.carbpol.2016.06.069
- Sato, R., Arita, T., Shimada, R., Nohara, T., Tabata, K., Koseki, K., Umemoto, K., and Masuhara, A. (2021). "Biocompatible composite of cellulose nanocrystal and hydroxyapatite with large mechanical strength," *Cellulose* 28(2), 871-879. DOI: 10.1007/s10570-020-03550-7
- Tang, Z., Kotov, N. A., Magonov, S., and Ozturk, B. (2003). "Nanostructured artificial nacre," *Nat. Mater.* 2, 413. DOI: 10.1038/nmat906
- Usuki, A., Kojima, Y., Kawasumi, M., Okada, A., Fukushima, Y., Kurauchi, T., and Kamigaito, O. (1993). "Synthesis of nylon 6-clay hybrid," *J. Mater. Res.* 8(5), 1179-1184. DOI: 10.1557/JMR.1993.1179
- Wang, Y. X., Tian, H. F., and Zhang, L. N. (2010). "Role of starch nanocrystals and cellulose whiskers in synergistic reinforcement of waterborne polyurethane," *Carbohydr. Polym.* 80(3), 665-671. DOI: 10.1016/j.carbpol.2009.10.043
- Wang, J. W., Gardner, D. J., Stark, N. M., Bousfield, D. W., Tajvidi, M., and Cai, Z. Y. (2018a). "Moisture and oxygen barrier properties of cellulose nanomaterial-based films," *ACS Sustain. Chem. Eng.* 6(1), 49-70. DOI: 10.1021/acssuschemeng.7b03523
- Wang, W. H., Zhang, X. L., Li, C., Du, G. H., Zhang, H. J., and Ni, Y. H. (2018b). "Using carboxylated cellulose nanofibers to enhance mechanical and barrier properties of collagen fiber film by electrostatic interaction," *J. Sci. Food Agric.* 98(8), 3089-3097. DOI: 10.1002/jsfa.8809
- Yang, J., Zhao, J. J., Han, C. R., Duan, J. F., Xu, F., and Sun, R. C. (2014). "Tough nanocomposite hydrogels from cellulose nanocrystals/poly(acrylamide) clusters: Influence of the charge density, aspect ratio and surface coating with PEG," *Cellulose* 21(1), 541-551. DOI: 10.1007/s10570-013-0111-4
- Yano, H., Sugiyama, J., Nakagaito, A. N., Nogi, M., Matsuura, T., Hikita, M., and Handa, K. (2005). "Optically transparent composites reinforced with networks of

- bacterial nanofibers," *Adv. Mater.* 17(2), 153-155. DOI: 10.1002/adma.200400597
- Yu, H.-Y., Zhang, H., Song, M.-L., Zhou, Y., Yao, J., and Ni, Q.-Q. (2017). "From cellulose nanospheres, nanorods to nanofibers: Various aspect ratio induced nucleation/reinforcing effects on polylactic acid for robust-barrier food packaging," *ACS Appl. Mater. Inter.* 9(50), 43920-43938. DOI: 10.1021/acsami.7b09102
- Yu, H. Y., and Yao, J. M. (2016). "Reinforcing properties of bacterial polyester with different cellulose nanocrystals *via* modulating hydrogen bonds," *Compos. Sci. Technol.* 136, 53-60. DOI: 10.1016/j.compscitech.2016.10.004
- Zhang, F. S., Zheng, X. T., Wang, C. L., Wang, D. D., Xue, X. Y., and Qing, G. Y. (2021). "Synthesis of optically active chiral mesoporous molybdenum carbide film," *J. Ind. Eng. Chem.* 94, 482-488. DOI: 10.1016/j.jiec.2020.11.023
- Zhang, H., She, Y., Song, S., Chen, H., and Pu, J. (2012). "Improvements of mechanical properties and specular gloss of polyurethane by modified nanocrystalline cellulose," *BioResources* 7(4), 5190-5199. DOI: 10.15376/biores.7.4.5190-5199
- Zhao, Q., Wei, Y. C., Ni, C. J., Wang, L. L., Liu, B. J., Liu, J., Zhang, M. Y., Men, Y. F., Sun, Z. Y., Xie, H. M., Hu, W., and Lu, Y. F. (2019). "Effect of aminated nanocrystal cellulose on proton conductivity and dimensional stability of proton exchange membranes," *Appl. Surf. Sci.* 466, 691-702. DOI: 10.1016/j.apsusc.2018.10.063

Article submitted: September 28, 2022; Peer review completed: October 29, 2022;
Revised version received and accepted: November 5, 2022; Published: November 16, 2022.

DOI: 10.15376/biores.18.1.447-464